Internal Sodium Ions and Water Molecules in Guanine Quadruplexes: Magnetic Relaxation Dispersion Studies of $[d(G_3T_4G_3)]_2$ and $[d(G_4T_4G_4)]_2$[†]

Karim Snoussi*[,‡] and Bertil Halle*

Department of Biophysical Chemistry, Center for Molecular Protein Science, Lund University, SE-22100 Lund, Sweden

Received August 31, 2008; Revised Manuscript Received September 28, 2008

ABSTRACT: The structural stability of guanine quadruplexes depends critically on an unusual configuration of dehydrated Na^+ or K^+ ions, closely spaced along the central axis of the quadruplex. Crystallography and NMR spectroscopy indicate that these internal ions can be located between the G-quartet planes as well as in the thymine loops, but the precise ion coordination has been firmly established in only a few cases. Here, we examine the bimolecular diagonal-looped foldback quadruplexes $[d(G_3T_4G_3)]_2$ (Q3) and $[d(G_4T_4G_4)]_2$ (Q4) by ^2H, ^{17}O, and ^{23}Na magnetic relaxation dispersion (MRD). The MRD data indicate that both quadruplexes contain Na^+ ions between the T_4 loops and the terminal G-quartets and that these ions have one water ligand. These ions exchange with external ions on a time scale of $10-60$ μs at 27 °C, while their highly ordered water ligands have residence times in the range $10^{-8}-10^{-6}$ s. The MRD data indicate that Q4 contains three Na^+ ions in the stem sites, in agreement with previous solid-state ^{23}Na NMR findings but contrary to the only crystal structure of this quadruplex. For Q3, the MRD data suggest a less symmetric coordination of the two stem ions. In both quadruplexes, the stem ions have residence times of 0.6−1.0 ms at 27 °C. The equilibrium constant for $Na^+ \rightarrow K^+$ exchange is ∼4 for both loop and stem sites in Q3, in agreement with previous ^1H NMR findings.

Guanine quadruplexes are nucleic acid structures built around a core of three or more stacked G-quartets, planar arrangements of four guanine bases linked by eight Hoogsteen H-bonds (*1, 2*). Quadruplex DNA appears to be involved in eukaryotic gene regulation and genomic stability (*3*), and G-quartets are of interest as building blocks in supramolecular chemistry (*4*). The structures of many DNA quadruplexes have been determined to near-atomic resolution by NMR spectroscopy or X-ray crystallography, but important questions remain concerning the energetics, stability, and dynamics of this structurally diverse nucleic acid class. A unique feature of the quadruplex structure is the presence of completely dehydrated alkali ions (usually K^+ or Na^+) coordinated to the buried carbonyl oxygens of the nucleotide bases. These internal ions are crucial for the stability and structural polymorphism of quadruplexes (*2, 5, 6*), but little is known about the energetics and kinetics of ion binding. In many cases, even the number of internal ions and their precise locations are under debate.

A variety of NMR spectroscopy and relaxation techniques can be used to probe the internal ions of quadruplexes in aqueous solution. The NH_4^+ (*7*) and Tl^+ (*8*) ions have been used as a spin-1/2 surrogates for the similarly sized K^+ ion, allowing direct observation, by ^1H or ^{205}Tl NMR, of internal ions in slow exchange with bulk ions. More recently, slowly exchanging internal ions have been observed by NMR spectroscopy of the quadrupolar (spin >1) nuclides ^{23}Na, ^{39}K and ^{87}Rb (*9, 10*). More rapidly exchanging internal ions can be studied via their effect on the quadrupolar spin relaxation rates associated with the dominant bulk-ion magnetization (*11−13*). As applied to quadruplexes, this NMR relaxation approach has so far been limited to line width measurements at a single resonance frequency (or magnetic field strength), making it difficult to separate contributions from external and internal ions and from different classes of internal ions. More detailed information about the internal ions can be obtained by measuring the spin relaxation rate(s) over a wide range of resonance frequencies. Such magnetic relaxation dispersion (MRD[1]) measurements have been used to study ion binding (via ^{23}Na relaxation) (*14, 15*) and hydration (via ^2H and ^{17}O relaxation) (*16, 17*) for *B*-DNA oligonucleotides. Here, we report the first MRD studies of quadruplex DNA, using the $^2H/^{17}O$ (for hydration) and ^{23}Na (for ion binding) nuclides.

We have chosen to study the bimolecular foldback quadruplexes formed by the oligodeoxyribonucleotides $d(G_3T_4G_3)$ (abbreviated Q3) and $d(G_4T_4G_4)$ (abbreviated Q4). The latter sequence contains the telomere repeat $d(T_4G_4)$ from the protozoan *Oxytricha nova*. These DNA oligomers form hairpins that dimerize head-to-tail to build a quadruplex with a central stem of three or four stacked G-quartets capped by diagonal T_4 loops. At least for Q4, this topology is formed with either Na^+, K^+, Tl^+ or NH_4^+ as internal ions, with only

[†] This work was supported by the Swedish Research Council, the Knut & Alice Wallenberg Foundation, the Crafoord Foundation, and the Wenner-Gren Center Foundation for Scientific Research.

* To whom correspondence should be addressed. (K.S.) Phone: + 32 10472777. Fax: +32 10479196. E-mail: Karim.Snoussi@uclouvain.be. (B.H.) Phone: +46 462229516. Fax: +46 46 2224543. E-mail: Bertil.Halle@bpc.lu.se.

[‡] Present address: Département de Chimie, Université catholique de Louvain, Place Louis Pasteur 1, B-1348 Louvain-la-Neuve, Belgique.

[1] Abbreviations: A_2T_2, d(CGCGAATTCGCG); DPF, dynamic perturbation factor; Q3, $d(G_3T_4G_3)$; Q4, $d(G_4T_4G_4)$; MRD, magnetic relaxation dispersion; QCC, quadrupole coupling constant.

10.1021/bi801657s CCC: $40.75
Published on Web 10/25/2008

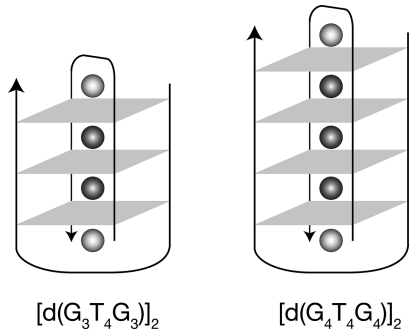

FIGURE 1: Schematic representations of the Q3 and Q4 quadruplexes, showing possible locations of internal ions in the stem (dark shading) and loop (light shading) regions.

minor structural variations. Even though Q4 has been studied extensively, ion binding to this quadruplex is not fully understood. Crystallography reveals five internal K^+ (*18*) or Tl^+ (*19*) ions: three are sandwiched between the G-quartet planes in the stem, and two are buried in the T_4 loops (Figure 1). According to ^{1}H NMR, NH_4^+ ions occupy the three stem sites, but are absent from the two loop sites (*20*−*22*). For the Na^+ form of Q4, the situation is less clear. The only crystal structure, where Q4 is complexed with a telomere-end-binding protein, shows four internal Na^+ ions asymmetrically located near (inner pair) or 1 Å outside (outer pair) the G-quartet planes (*23*). In contrast, solid-state ^{23}Na NMR indicates that Q4 contains three Na^+ ions sandwiched between the G-quartets in the stem (*24*), and an additional slow-exchange peak (observed at low temperatures) in the solution ^{23}Na NMR spectrum was assigned to two Na^+ ions in the loop sites (*10*). It thus appears that Na^+ and K^+ ions occupy the same internal sites in Q4 (Figure 1) and that the different internal-Na^+ configuration seen in the quadruplex−protein complex may be induced by the protein or by other crystal-specific interactions.

For the Q3 quadruplex, less is known about the internal ions. No crystal structure is available, but the NMR solution structure of the Na^+ form of Q3 (*25*) has the same diagonal-looped foldback topology as for Q4, but without the 2-fold symmetry (*26, 27*). The solution structure of the K^+ form of Q3 shows multiple loop conformations, but is otherwise very similar to the Na^+ form (*28*). The nonmonotonic variation of ^{1}H NMR shifts on replacing Na^+ by K^+ indicates at least two internal-ion sites in Q3 (*29*), but, on the basis of analogy with Q4, it has been argued (*10*) that Q3 contains four internal ions (Figure 1).

The internal ions in guanine quadruplexes are not static but exchange with external ions. Because of the high stability imparted by multiple interstrand H-bonds within the G-quartets, the integrity of the quadruplex structure is maintained on the subsecond time scale of ion exchange, as indicated by the much slower imino proton exchange (*30*). The quadruplex thus constitutes an ion channel, where internal ions exchange via the terminal loops rather than directly via the grooves (*20*). The kinetics of internal-ion exchange can aid in the assignment of binding sites and provides information about conformational fluctuations. For the Q4 quadruplex, ^{23}Na NMR indicates that the Na^+ ions in the loops exchange on a time scale of $\sim 10^{-4}$ s (*10*), while the stem ions exchange more slowly. For the Q3 quadruplex, ^{1}H NMR shows that coexisting Na^+ and K^+ forms are in fast exchange on the ^{1}H chemical shift time scale of ~10 ms (*29*). The present ^{23}Na MRD analysis sheds new light on the internal ions in these two quadruplexes.

DNA−water interactions are important for stability, dynamics, and recognition by proteins and drugs. For *B*-DNA, a considerable body of knowledge has accumulated about hydration structure (*31*), hydration dynamics (*32*), and water involvement in recognition (*33*). Much of this work has focused on the ordered hydration motif found in the minor groove of AT-tracts (*34*). The most important aspect of quadruplex hydration is perhaps the dehydration of internal ions, which is thought to control the relative affinity of different monovalent ions for the internal sites (*29*). Whereas stem ions are completely dehydrated, loop ions may retain one or two water ligands. In the loop sites of Q4, it appears that K^+ prefers to have two water ligands (*18*), whereas Na^+ coordinates a single water molecule (*23*). For Q3, no information about ion−water coordination is available. Beyond the time-averaged static picture provided by crystallography, virtually nothing is known about quadruplex hydration. The ^{2}H MRD data presented here provide information about loop-ion hydration and water exchange kinetics, as well as about the hydration dynamics of the grooves and phosphodiester backbones.

EXPERIMENTAL PROCEDURES

Sample Preparation. The oligodeoxyribonucleotides $d(G_3T_4G_3)$ (Q3) and $d(G_4T_4G_4)$ (Q4) were synthesized on a 50 μmole scale, purified by HPLC, and dialyzed against NaCl at Oligos Etc. (Wilsonville, OR). The purity of these preparations, determined by analytical anion-exchange HPLC at Scandinavian Gene Synthesis (Köping, Sweden) was 96.8% (Q3) and 97.2% (Q4). To remove traces of other counterions, the oligonucleotides were successively dialyzed against 2, 0.5, and 0.1 M NaCl(aq) and then twice against Millipore water. DNA solutions were prepared at strand concentrations of 2.58 mM (Q3) or 2.06 mM (Q4) by dissolving the lyophilized oligonucleotides in a mixture of 50% $H_2{}^{17}O$ (19.2 atom% ^{17}O) and 50% D_2O (with low paramagnetic content), adding NaCl to 200 mM and adjusting pH to 6.2 (not corrected for isotope effects). The reference sample contained 200 mM NaCl in the same water mixture as that used for the DNA samples. The strand concentration was determined from the absorbance at 260 nm (measured after serial dilution to the μM range, heating to 90 °C for 5 min and rapid cooling to room temperature), using an extinction coefficient of 0.950×10^5 M^{-1} cm^{-1} (Q3) or 1.152×10^5 M^{-1} cm^{-1} (Q4), as given by the nearest-neighbor model (*35*). To form the quadruplex, the DNA solutions were heated to 90 °C for 5 min, slowly cooled to room temperature, and kept at 4 °C overnight. Before and after the MRD measurements, the presence of the expected quadruplex structure was confirmed by recording one-dimensional ^{1}H spectra at 500 and 600 MHz (on Varian Inova spectrometers). The spectra, taken at 20, 25, and 27 °C, were found to match the published spectra from the bimolecular foldback quadruplexes of Q3 (*26, 27, 29*) and Q4 (*7, 21, 30*). The ion competition experiments were then performed after successive additions of KCl to 100, 200, and 400 mM. On the basis of literature data (*26, 36, 37*), we estimate the quadruplex melting temperature in our samples to ~50 °C for Q3 and

~70 °C for Q4. Addition of KCl will increase these temperatures (*38*).

^{23}Na MRD Measurements. The relaxation rates, R_1 and R_2, of the longitudinal and transverse ^{23}Na magnetization, respectively, were measured at 11 magnetic field strengths in the range of 0.38−14.1 T, corresponding to ^{23}Na resonance frequencies of 4.28−159 MHz. To cover this range, we used Tecmag Discovery or Apollo consoles equipped with field-variable iron-core magnets (4.28−20.6 MHz), Bruker Avance DMX 100 and 200 (26.5 and 52.9 MHz), and Varian Inova 360, 500 and 600 (95.7, 132 and 159 MHz) spectrometers with conventional cryomagnets. Each inversion−recovery (R_1) or spin−echo (R_2) relaxation experiment comprised 20−40 variable-delay spectra with signal-to-noise ratio >100, requiring accumulation of up to 6×10^4 transients per spectrum. The 90° pulse length was <15 μs, and an acquisition delay of 100−250 μs was used to suppress acoustic ringing at frequencies <15 MHz. Pulse amplitude and phase imperfections were compensated by standard phase cycling. All spectra were Fourier transformed and phase- and baseline-corrected, and the peak was integrated between points where the peak intensity had dropped well below the noise level. All reported MRD measurements were performed at a temperature of 27.0 °C, regulated to within ± 0.1 °C with a thermostatted air flow and measured with a copper−constantan thermocouple in a dummy sample. The 1.0 mL MRD samples were contained in 10-mm quartz tubes. The ^{23}Na relaxation rates of the reference sample (200 mM NaCl aqueous solution) was measured at all field strengths, yielding $R^0 = 18.3 \pm 0.4$ s^{-1}. Because R^0 does not depend on the resonance frequency, these reference measurements also served as an additional temperature check. Being a spin-3/2 nuclide, ^{23}Na has intrinsically biexponential relaxation. In practice, however, biexponentiality is rarely observed except for transverse relaxation at high frequencies. In the present study, nearly all relaxation decays were monoexponential within the experimental accuracy of 1−2%. We thus obtained the effective longitudinal and transverse relaxation rates $R_1^{\S}$ and $R_2^{\S}$. A significant biexponentiality was observed only at the two highest frequencies (132 and 159 MHz), where a 5-parameter fit yielded the two transverse rates R_2^- and R_2^+. Within the experimental accuracy, the calculated effective rate, $R_2 = 0.4\,R_2^- + 0.6\,R_2^+$, did not differ from the rate, $R_2^{\S}$, obtained directly from a monoexponential fit to the magnetization data.

^{2}H and ^{17}O MRD Measurements. The relaxation rates of the water ^{2}H and ^{17}O magnetizations were measured on the same samples as those used for the ^{23}Na experiments and using the same pulse sequences as for ^{23}Na. The ^{2}H, ^{17}O, and ^{23}Na measurements were performed sequentially at each magnetic field strength. The accessed frequency range was 2.48−92.1 MHz for ^{2}H and 2.19−81.3 MHz for ^{17}O. Modulation of the ^{1}H−^{17}O and ^{2}H−^{17}O scalar spin couplings by hydrogen exchange among water molecules (on the millisecond time scale at pH 6.2) gives rise to a large scalar relaxation contribution to $R_2(^2\text{H})$ and $R_2(^{17}\text{O})$ (*39*). In addition, hydrogen-exchange modulation of the ^{17}O chemical shift difference among the isotopic species H_2O, HDO, and D_2O contributes to $R_2(^{17}\text{O})$ at high magnetic fields (*39*). Under these conditions, useful information about quadruplex hydration can only be deduced from the R_1 data, which are free from these complications. The ^{2}H and ^{17}O relaxation rates of the reference sample were measured at all field strengths, yielding $R^0(^2\text{H}) = 2.02 \pm 0.01$ s^{-1} and $R^0(^{17}\text{O}) = 150.6 \pm 0.1$ s^{-1}.

Quadruplex Rotational Diffusion. To obtain the rotational correlation time τ_R of the quadruplexes, we performed hydrodynamic calculations with the program HYDROPRO v. 7c (*40*). The primary hydrodynamic model contained 420 (Q3) or 510 (Q4) nonhydrogen atoms, all of which were given an effective hydrodynamic radius of 3.0 Å (*40, 41*). In the calculations, this model was replaced by a shell of smaller beads of radius σ. The rotational diffusion tensor $\mathbf{D}_R$ was computed as a function of σ and extrapolated to $\sigma = 0$ by using 7 σ values in the range 0.75−1.60 Å. The rank-2 isotropic rotational correlation time is defined as $\tau_R = (2\ \text{Tr}\ \mathbf{D}_R)^{-1}$. For the Na^+ form of the Q3 quadruplex, we obtained $\tau_R = 3.09$ ns as an average over the first 3 models in the NMR structure 1FQP (*25*). For the Q4 quadruplex, we obtained $\tau_R = 3.47$ ns for the crystal structure 1JB7 (*23*) of the Na^+ form and $\tau_R = 3.56$ ns for the K^+ form crystal structures 1JRN and 1JPQ (*18*). The NMR structures 156D (Na^+ form) (*42*) and 1K4X (K^+ form) (*21*) of Q4 yield $\tau_R = 3.70$ and 3.32 ns, respectively, in both cases averaged over the first three NMR models. All of these τ_R values pertain to 27 °C and the viscosity (0.956 cP) of our solvent. For the analysis of our MRD data at 27 °C, we used $\tau_R = 3.1$ and 3.5 ns for Q3 and Q4, respectively. In all cases, the rotational anisotropy is negligibly small, with values of 1.05−1.10 for the ratio of the largest and smallest of the five rotational correlation times (derived from the three eigenvalues of $\mathbf{D}_R$) that characterize the rank-2 spectral density function for asymmetric-top rotational diffusion. The effect of electrolyte friction was neglected since it can be estimated to increase τ_R by at most a few percent in our samples (Stuart Allison, personal communication).

RESULTS

Water ^{2}H MRD Results. Because of the low concentration (~1 mM) and short tumbling times (3−4 ns) of the quadruplexes, the water ^{2}H or ^{17}O relaxation rate R_1 exceeds the relaxation rate R^0 of the bulk solvent by only 2−10% (depending on the resonance frequency). For this reason, we focus here on the somewhat more accurate ^{2}H results. The corresponding analysis of the ^{17}O data yields similar model parameter values, indicating that labile DNA hydrogens make little or no contribution to $R_1(^2\text{H})$ at pH 6.2 and 27 °C. A previous water ^{2}H and ^{17}O MRD study of a *B*-DNA dodecamer duplex also indicated negligible contribution from labile DNA hydrogens (*16*).

The ^{2}H MRD profiles for Q3 and Q4 (Figure 2) are modeled with the usual fast-exchange expression (*39*)

$$R_1(\omega_0) - R^0 = \alpha + \beta\tau_C\left[\frac{0.2}{1+(\omega_0\tau_C)^2} + \frac{0.8}{1+(2\omega_0\tau_C)^2}\right] \quad (1)$$

where $\omega_0 = 2\pi\nu_0$ is the angular resonance frequency. The parameter $\alpha = (N_H/N_W)\,R^0(\xi_H - 1)$ describes the frequency-independent contribution from subnanosecond water rotation in the hydration layer of the quadruplex. Here, N_W (5.5×10^4 for 1 mM quadruplex) is the water/quadruplex mole ratio in the sample, and $R^0 = 2.02$ s^{-1} is the relaxation rate in a bulk solvent reference sample. Furthermore, N_H is the number of water molecules in the hydration layer, and

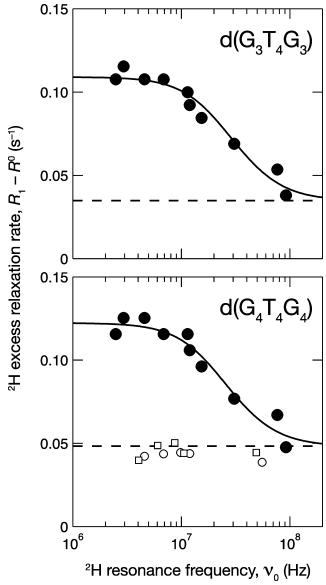

FIGURE 2: Water ^{2}H MRD profiles of Q3 (top) and Q4 (bottom) at pH 6.2, 27 °C, and 200 mM NaCl. The data have been normalized to 1.0 mM quadruplex using the fact that $R_1 - R^0$ is proportional to the quadruplex concentration; see eq 1. Each solid curve resulted from a 2-parameter fit to eq 1, with α indicated by the dashed line. The open symbols in the lower panel are ^{2}H (circles) and ^{17}O (squares) $R_1 - R^0$ data for the *B*-DNA duplex [d(CGCGAATTCGCG)]$_2$ at pH 6.5 and 27 °C (*16*), scaled to 1 mM duplex.

the dynamic perturbation factor (DPF) $\xi_H = \langle\tau_H\rangle/\tau_0$, the ratio of the water rotational correlation times in the hydration layer (averaged over the quadruplex surface) and in bulk solvent, is a global measure of hydration dynamics (*43*). The parameter $\beta = (N_I/N_W)(\omega_Q S_I)^2$ is associated with hydration water molecules with residence time $\tau_I > 1$ ns, as required to observe a frequency dependence in R_1 in the accessible frequency range ($\nu_0 < 100$ MHz). Such long-lived water molecules are invariably trapped in cavities or deep pockets, and they are therefore referred to as internal water molecules. In the expression for β, $\omega_Q = 8.7 \times 10^5$ s^{-1} (*39*) is the nuclear quadrupole frequency of a water deuteron, and S_I is the root-mean-square orientational order parameter for the N_I internal water molecules. Finally, the correlation time is $\tau_C = (1/\tau_R + 1/\tau_I)^{-1}$, with τ_R the rotational correlation time of the quadruplex.

The observation of a clear frequency dependence in R_1 (Figure 2) demonstrates that these quadruplexes contain internal water molecules with residence times in the nanosecond range or longer. The fits shown in Figure 2 were performed with the correlation time τ_C fixed at the quadruplex tumbling time obtained from molecular hydrodynamics calculations on the reported quadruplex structures: $\tau_R = 3.1$ and 3.5 ns for Q3 and Q4, respectively (see Experimental Procedures). Because the observed dispersions conform to these correlation times, we conclude that the β term in eq 1 is produced by water molecules with residence time $\tau_I \gg 3$ ns at 27 °C. The fit yields $N_I S_I^2 = 1.7 \pm 0.2$ for Q3 and 1.5 ± 0.2 for Q4. Since $S_I^2 \leq 1$, it follows that each quadruplex contains at least 2 internal water molecules. An upper bound on the residence time of these internal water molecules is provided by the fast-exchange condition: $(\omega_Q S_I)^2 \tau_C \tau_I \ll 1$ (*39*). We can thus conclude that $\tau_I \ll 1$ ms. However, a more restrictive upper bound is provided by the ^{17}O MRD data (not shown) from the same samples: $\tau_I \ll 10$ μs. The α parameter deduced from the fit yields $N_H(\xi_H - 1) = (1.0 \pm 0.2) \times 10^3$ for Q3 and $(1.3 \pm 0.2) \times 10^3$ for Q4. We expect the hydration number N_H to be proportional to the solvent-accessible surface area A_S of the quadruplex. For the same quadruplex structures as those used for the τ_R calculation (see Experimental Procedures), we obtain (with a probe radius of 1.4 Å) $A_S = 3400$ Å^2 for Q3 and 3830 Å^2 for Q4. Adopting the same value as that determined for proteins and small solutes, 10.75 Å^2, for the accessible surface area occupied per water molecule on average (*43*), we find $N_H = 316$ for Q3 and 356 for Q4. With these N_H values, we can deduce the DPF: $\nu_H = 4.0 \pm 0.5$ for Q3 and 4.7 ± 0.6 for Q4.

Sodium Ion ^{23}Na MRD Results. The analysis of the effective (single-exponential) ^{23}Na relaxation rates R_1 and R_2 is more involved than that for the water ^{2}H data. First, we cannot assume fast-exchange conditions since the residence times of the internal Na^+ ions are expected (*10, 13, 29*) to be similar to or longer than the intrinsic ^{23}Na relaxation time of a bound Na^+ ion, estimated to 50−100 μs. Second, we must allow for at least two types of internal Na^+ ions, residing in stem sites (between the G-quartets) and in loop sites (between the T_4 loop and the terminal G-quartet); see Figure 1. After these generalizations, the longitudinal ^{23}Na relaxation rate can be expressed as (*15*)

$$R_1(\omega_0) - R^0 = \alpha + \sum_k \hat{\beta}_k \hat{\tau}_{C,k} \left[\frac{0.2}{1 + (\omega_0 \hat{\tau}_{C,k})^2} + \frac{0.8}{1 + (2\omega_0 \hat{\tau}_{C,k})^2} \right] \quad (2)$$

with a similar expression for R_2 (*15*). In addition, R_2 contains a contribution from exchange modulation of the chemical shift difference between internal and external Na^+ ions. However, depending on the ion exchange rate, this shift difference may be partly refocused by the spin echo pulse sequence used here to measure R_2. Because of this complication, and since R_2 data are generally less accurate than R_1 data, we include only R_1 data in the fits.

In eq 2, α has the same meaning as in eq 1, except that N_W is replaced by N_{Na}, the Na^+/quadruplex mole ratio in the sample (220 for 1 mM quadruplex). The effective β amplitude parameter $\hat{\beta}_k$ and the effective correlation time $\hat{\tau}_{C,k}$ are given by (*15*)

$$\hat{\beta}_k = \frac{\beta_k}{[1 + R_k(0)\tau_k]^{1/2}} \quad (3)$$

$$\hat{\tau}_{C,k} = \frac{\tau_{C,k}}{[1 + R_k(0)\tau_k]^{1/2}} \quad (4)$$

where $\beta_k = (N_{I,k}/N_{Na})(\omega_{Q,k} S_{I,k})^2$ and $\tau_{C,k} = (1/\tau_R + 1/\tau_k)^{-1}$, in analogy with the ^{2}H case, and $R_k(0) = (\omega_{Q,k} S_{I,k})^2 \tau_{C,k}$ is the intrinsic ^{23}Na relaxation rate at $\omega_0 = 0$ of a (nonexchanging) ion in site *k*. In practice, $\tau_{C,k} = \tau_R$ since the internal-ion residence times $\tau_{I,k}$ are much longer than the quadruplex tumbling time τ_R. For ^{23}Na, it is customary to specify the quadrupole coupling constant (QCC) χ_Q, rather then the quadrupole frequency ω_Q. If we subsume the asymmetry factor $(1+\eta^2/3)^{1/2}$ into the QCC, these quantities are related as $\omega_Q = (2/5)^{1/2} \pi \chi_Q$.

In principle, Na^+ ions in the external counterion sheath could also contribute to the observed ^{23}Na relaxation disper-

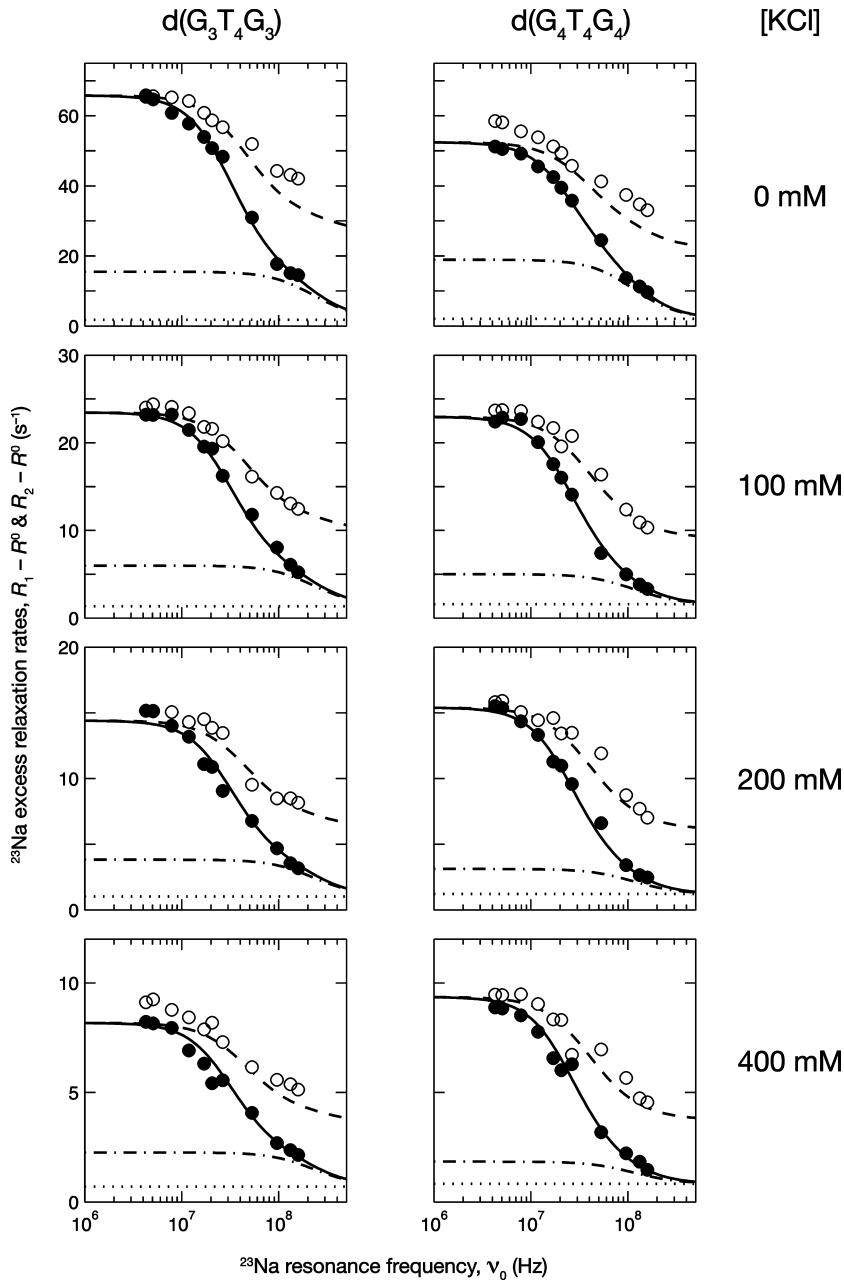

FIGURE 3: ^{23}Na R_1 (○) and R_2 (●) dispersion profiles of Q3 (left column) and Q4 (right column) at pH 6.2, 27 °C, and 200 mM NaCl. The data have been normalized to 1.0 mM quadruplex using the fact that $R_1 - R^0$ is proportional to quadruplex concentration; see eq 2. The four rows of panels (with different scales on the *y* axis) correspond to different KCl concentrations as indicated. For each quadruplex, the solid curves resulted from a global fit to the four sets of R_1 data using eq 2 with two classes of internal-ion sites. Also indicated for each sample are α (dotted line) and the R_1 profile without contributions from loop ions (dash-dotted curve).

sion. However, in the case of *B*-DNA, the Na^+−phosphate interactions are diffuse and short-lived (*15, 44*) and therefore cannot give rise to residence times ≫ 3 ns and QCCs of ∼1 MHz (as expected for internal ions). This should be the case also for quadruplex DNA. In eq 2, we therefore describe the effect of Na^+ ions in the counterion sheath by the small, frequency-independent term α.

Figure 3 shows ^{23}Na MRD profiles for 8 samples containing 220 mM Na^+ (200 mM added NaCl plus neutralizing external counterions) in addition to 0, 100, 200, or 400 mM KCl. All dispersion profiles are significantly more stretched than would be the case for a single correlation time. The model must therefore contain at least two internal ion sites, described by β terms with $k = 1$ and $k = 2$ in eq 2. The model was implemented in a global fit to the four R_1 dispersion profiles for each quadruplex. For this analysis, we assume that the only effect of KCl addition is to replace Na^+ ions by K^+ ions at the internal sites as well as in the external counterion sheath. The internal sites are assumed to be fully occupied (strong binding limit) by either Na^+ or K^+. Since at most a few percent of the ions are internally bound, the parameter β_k then depends on the K^+ and Na^+ concentrations as

$$\beta_k(C_K) = \frac{\beta_k(0)}{1 + K_k C_K / C_{Na}} \quad (5)$$

where K_k is the equilibrium constant for the process where one Na^+ ion is replaced by one K^+ ion at internal site *k*. Equation 5 is strictly valid only for equivalent and independent sites; therefore, K_k should be regarded as an effective

Table 1: Parameter Values from Global Fits to ^{23}Na MRD Data[a]

parameter	d($G_3T_4G_3$)	d($G_4T_4G_4$)
χ_{stem} (MHz)	2.8 ± 0.6	1.3 ± 0.1
τ_{stem} (ms)	0.7 ± 0.1	0.8 ± 0.2
K_{stem}	4.2 ± 0.5	9 ± 2
χ_{loop} (MHz)	0.75 ± 0.07	0.54 ± 0.06
τ_{loop} (μs)	40 ± 20	25 ± 35
K_{loop}	4.0 ± 0.2	1.9 ± 0.2

[a] Parameter errors correspond to one standard deviation.

exchange constant. In the external counterion sheath, we assume that Na^+ and K^+ ions are present in the same proportion as in the bulk solvent so that

$$\alpha(C_K) = \frac{\alpha(0)}{1 + C_K/C_{Na}} \quad (6)$$

To reduce the number of freely adjustable parameters (4 per internal ion site), we impose constraints based on prior knowledge. Unconstrained fits yield reasonable parameter values, but some of the covariances are large. The α term makes only a small contribution to R_1 (Figure 3), and we fixed the dimensionless parameter $\alpha_{red} \equiv C_{Na}\,\alpha(0)/(C_Q\,R^0)$ to 25 s^{-1} for Q3 and 30 s^{-1} for Q4. The Q4 value is based on unconstrained fits (the Q4 data extend to lower R_1 values and therefore determine α_{red} more precisely) and the Q3 value follows from the expectation that α_{red} is proportional to the structural charge of the quadruplex (internal ions included), i.e., $\alpha_{red}(Q3) = (14/17)\,\alpha_{red}(Q4)$. These α_{red} values are similar to the value, 26 s^{-1}, obtained for a *B*-DNA dodecamer duplex under similar conditions (*15*). For both quadruplexes, unconstrained fits yield one internal-ion class in slow exchange (τ_1 of order 1 ms) and another class in fast-to-intermediate exchange ($\tau_2 < 100\ \mu$s). On the basis of prior knowledge about the exchange kinetics of internal Na^+ ions in Q3 and Q4 (*10, 13, 29*), we identified these classes with sites between the G-quartets in the quadruplex stem ($k = 1$) and with sites between the T_4 loops and the terminal G-quartets ($k = 2$). In the following, we refer to these classes as stem and loop sites, respectively. The number and location of internal ions in quadruplexes have been controversial, but recent solid-state and solution ^{23}Na NMR spectroscopy indicates 3 stem sites and 2 loop sites in Q4 (*10, 24*), as depicted in Figure 1. By analogy, there should be 2 stem sites and 2 loop sites in Q3 (*10*).

The global fits to the 44 R_1 values for each quadruplex yield the solid curves in Figure 3 and the parameter values in Table 1. The stem ions, with residence times close to 1 ms, are in the slow-exchange regime, $R_{stem}(0)\,\tau_{stem} > 10$. As a result, the amplitude parameter $\hat{\beta}_{stem}$ and the effective correlation time $\hat{\tau}_{C,\,stem}$ are both reduced by a factor 4−8; see eqs 3 and 4. The stem-ion contribution to the R_1 dispersion profile (dash-dotted curve in Figure 3) is thus attenuated by 1−2 orders of magnitude at low frequencies, while the inflection point is upshifted in frequency by a factor 4−8 as compared to the fast-exchange condition. The loop-ion contribution, which dominates R_1 at low frequencies, is in the fast-to-intermediate-exchange regime, with $R_{loop}(0)\,\tau_{loop} < 0.1$ and $\hat{\tau}_{C,\,loop}$ only 5−10% below τ_R. Because the deviation from the fast-exchange limit is small, the residence time τ_{loop} is not accurately determined: for both quadruplexes, the data are consistent with τ_{loop} in the range 10−60 μs. The QCCs are all of the order 1 MHz, as expected (*24*), and the exchange constants *K* are in the range 2−10, consistent with previous results (*29*). These results are discussed in more detail below.

As seen from Figure 3, the R_2 dispersion profiles (dashed curves) calculated with the parameter values obtained from the fit to the R_1 data agree rather well with the measured R_2 data, supporting our analysis. The minor discrepancies may be attributed to experimental artifacts and to a partly quenched (by the spin echo sequence) contribution from chemical shift modulation (at high frequencies).

DISCUSSION

Internal Ion Sites. Our ^{23}Na MRD analysis is based on the assumption (*10*) that the quadruplexes have two loop sites and two (Q3) or three (Q4) stem sites (Figure 1), all of which are fully occupied by Na^+ or K^+ ions. If these assumptions are correct, then the values of the QCC χ, the exchange constant *K*, and the residence time τ_1 derived from the fit must be consistent with prior knowledge about these quantities. For the K^+ form of Q4, five internal ions have been detected crystallographically (*18*). For the Na^+ form of Q4, solid-state and solution ^{23}Na NMR spectroscopy indicates five internal ions (*10, 24*), whereas a crystal structure of a protein-associated quadruplex detects only four internal ions (*23*). For Q3, the number of internal ions is unknown, but a four-ion configuration has been postulated by analogy with Q4 (*10*).

The QCC reflects the coordination geometry and symmetry of the ionic site and is typically in the range 1−3 MHz for Na^+ ions coordinated to 5−8 oxygen atoms (*24, 45, 46*). For the three stem ions in Q4, the QCC has been determined by solid-state ^{23}Na NMR: $\chi_{stem} = 1.2 \pm 0.2$ MHz (*24*). This value, which incorporates the asymmetry factor (see above) and is rms averaged over the inner and outer stem sites (as appropriate for our relaxation data), agrees quantitatively with our result: $\chi_{stem} = 1.3 \pm 0.1$ MHz. These ions are thought to be located between the G-quartet planes, with square antiprism coordination to the 8 G.O6 atoms from the two adjacent G-quartets (*24*). For the 2 putative stem sites in the Q3 quadruplex, we obtain a larger QCC, $\chi_{stem} = 2.8 \pm 0.6$ MHz, indicating a less symmetric coordination. The Q3 quadruplex lacks the 2-fold symmetry of Q4 (*26, 27*); therefore, the two stem sites are not equivalent. QCC values of ∼3 MHz have been reported for Na^+ ions in pentacoordinated square-pyramidal and hexacoordinated distorted trapezoidal bipyramidal geometry (*46*). The locations of the internal ions in Q3 have not been established. Interestingly, the ion channel is wider in Q3 than in Q4, with mean diagonal G.O6−G.O6 separations of 4.94 and 4.19 Å, respectively. These values were obtained by averaging over the first three models in the NMR structures of the Na^+ form of the quadruplexes (*25, 42*). This widening of the Q3 channel may indicate that the Na^+ ions approach the G-quartet planes more closely than in Q4 and would then be consistent with the larger QCC.

In the crystal structure of the Na^+ form of Q4, there are only two stem ions, located ∼0.5 Å outside the two central G-quartet planes (*23*). This internal-ion configuration is not consistent with solid-state ^{23}Na NMR, which indicates that three stem ions are sandwiched between the four G-quartet planes (*24*). The different ion configuration in the crystal

structure may be caused by interactions with the telomere end binding protein also present in this crystal (*23*), or it may be a cryoartifact. All quadruplex crystal structures discussed here have been determined at 100 K, and re-equilibration of ion and water positions may well occur on the millisecond time scale of flash cooling (*47*). As noted before (*24*), the crystal structure also deviates in that G-quartets are not stacked coaxially. A line connecting the internal ions is thus tilted by ~22° with respect to the normals to the two central (most planar) G-quartets (*23*). With a G-quartet separation of 3.3 Å. this tilt angle corresponds to 1.3 Å relative lateral displacement of adjacent G-quartets, which makes a central ion location less favorable energetically. Because the stem ions are in the slow-exchange regime, only two of the three parameters N_{stem}, χ_{stem} and $\tau_{I,stem}$ are independent. Virtually identical fits are thus obtained for other N_{stem} values, but with the other two parameters scaled as $\chi_{stem} \propto 1/(N_{stem})^{1/2}$ and $\tau_{I,stem} \propto N_{stem}$. For example, setting $N_{stem} = 2$ (rather than 3) for Q4 yields $\chi_{stem} = 1.6 \pm 0.1$ MHz, which does not agree with the solid-state ^{23}Na NMR result (*24*).

For the putative loop sites, we obtain smaller QCCs in the range 0.5−0.8 MHz (Table 1). These values are smaller than the static QCCs usually found for Na^+ ions in ordered environments (*24, 45, 46*). The loop Na^+ ions are thought to be coordinated to the four G.O6 atoms of the terminal G-quartet and to two T.O2 atoms from the T_4 loop (Q3) or to one T.O2 atom and one semiburied water molecule (*10*). The small QCC is thus not likely to result from a highly symmetrical coordination geometry. Instead, we attribute the QCC reduction to structural disorder in the loops. The QCC that governs the ^{23}Na relaxation and that we simply denote by χ is really a double time average that may be expressed as $\langle\langle\chi\rangle_\tau^2\rangle_k^{1/2}$. The first average is over motions faster than the quadruplex tumbling time τ_R (3−4 ns). This average plays the same role as the orientational order parameter S_I for internal water molecules, but now, both the orientation of the electric field gradient tensor and its principal values are averaged. The second average involves the spin relaxation rate and therefore the square of the QCC; it extends over all conformations and sites sampled by the ion on the spin relaxation time scale (~100 μs). Several studies indicate structural disorder that may be linked to the inferred QCC averaging in the loop sites. Flexibility in the T_4 loops of Q4 is indicated by distinct conformational differences in the loops of the Na^+ and K^+ forms (*21*) and by modulation of the ^{1}H chemical shift of the methyl protons of T5 in the Tl^+ form on a time scale of 0.34 ms at 10 °C (*19*). For the K^+ form of Q3, the solution structure shows multiple loop conformations, and molecular simulations indicate substantial conformational fluctuations in the loops on the subnanosecond time scale (*28*). The premelting transition reported for Q4 at temperatures above ~30 °C (*37, 48, 49*) has been attributed to conformational changes in the T4 loops (*37*). In fact, preliminary ^{23}Na MRD data at 45 °C (not shown) appear to be consistent with a loss of the loop ions in the premelting transition.

Internal Ion Exchange. The mean residence times of the internal Na^+ ions deduced from the ^{23}Na MRD data are essentially the same for Q3 and Q4: $\tau_{I,stem} = 0.6-1.0$ ms and $\tau_{I,loop} = 10-60$ μs at 27 °C. The similarity of the residence times for Q3 and Q4 is consistent with similar locations of the internal ions in the two quadruplexes. In particular, it supports the hypothesis that Q3 also contains loop-coordinated Na^+ ions (*10*).

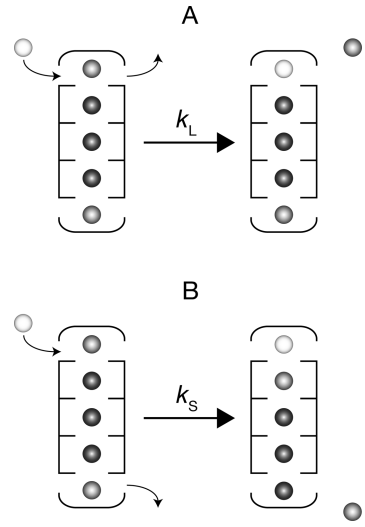

FIGURE 4: Schematic view of the two internal-ion exchange mechanisms in the Q4 quadruplex: (A) direct exchange at the loop site and (B) stepwise displacement of the ion file.

The 1−2 orders of magnitude faster exchange of the loop ions as compared to the stem ions is understandable on the basis of the quadruplex structure. If all internal-ion sites are fully occupied and if exchange cannot take place directly from stem sites, then there are two possible exchange mechanism (Figure 4). In the first mechanisms, an external ion directly replaces a loop ion without affecting the other internal ions. In the second mechanism, an external ion enters a loop site and pushes the file of ions one step through the channel so that the loop ion at the other end of the quadruplex exits into solution. A sequence of such concerted file displacements triggered by external ion intrusion at either loop site may be modeled as a symmetric random walk. The rate constants, k_L and k_S, for the two mechanisms are pseudofirst-order since the counterion concentration near the quadruplex may, to a first approximation, be regarded as constant independent of the total ion concentration. Loop ions can exchange by either mechanism so that $\tau_{I,loop} = 1/(k_L + k_S)$. A stem ion must first move to a loop site by one or more S-processes, whereafter it exchanges like a loop ion. Thus, $\tau_{I,stem} = m/k_S + 1/(k_L + k_S)$, where $m = 1$ for Q3, while $m = 3$ for the central site and 2 for the outer stem sites in Q4. These m coefficients follow from a calculation of the mean-first-passage time for a sequence of S-processes (*50*). If the three stem sites in Q4 are treated as equivalent, then the average $\tau_{I,stem}$ corresponds to $m = 7/3$. On physical grounds, we expect that $k_L \gg k_S$, in which case $\tau_{I,loop} = 1/k_L$ and $\tau_{I,stem} = m/k_S$ with $m = 1$ for Q3 and $m = 7/3$ for Q4. It then follows that $\tau_{I,stem} \gg \tau_{I,loop}$, as deduced from the ^{23}Na MRD data. The finding that $\tau_{I,stem}$ is the same for Q3 and Q4 thus indicates that the factor 7/3 is offset by a similar difference in k_S between the quadruplexes.

By suppressing the bulk Na^+ signal, Ida and Wu were able to directly observe at 5 °C two ^{23}Na signals from slowly exchanging Na^+ ions assigned to the stem and loop sites in Q4 (*10*). By identifying the disappearance of the loop peak at 15 °C with the coalescence of the bulk and loop peaks, they deduced $\tau_{I,loop} = 0.22 \pm 0.03$ ms at this temperature

(*10*). Alternatively, one may derive the residence time from the exchange-broadening of the loop peak. Using parameter values from the present study to estimate the intrinsic line width (and dynamic shift), we find from the reported linewidths at 5 and 10 °C (*10*) that $\tau_{I,loop} = 0.55$ ms at 5 °C and 0.35 ms at 10 °C. This corresponds to an activation energy of 56 kJ mol^{-1}, implying that $\tau_{I,loop}$ is 0.23 ms at 15 °C, in agreement with the coalescence-based estimate (*10*), and 90 μs at 27 °C, not far from our value. The roughly 2-fold shorter $\tau_{I,loop}$ obtained here may be related to the higher Na^+ concentration in our sample (220 vs 70 mM), which might increase the pseudo-first-order exchange rate constant k_L by increasing the attempt frequency (proportional to the Na^+ concentration outside the loops) or by lowering the energy barrier (by Debye screening). We note that the intrinsic line width that we have calculated pertains to the narrow component (which does not involve the zero-frequency spectral density); the broad component is predicted to have a line width of ~2 kHz and would thus merge with the baseline even at 5 °C.

Deng and Braunlin estimated the internal Na^+ residence time in Q4 from the exchange broadening of the bulk-Na^+ peak, obtaining a value of 0.25 ms at 10 °C (*13*). This value is close to the 0.35 ms deduced from the exchange broadening of the loop-ion peak (see above), but this agreement is likely to be fortuitous. Indeed, the results at 10 and 30 °C reported by Deng and Braunlin imply an activation energy of only 22 kJ mol^{-1}. In their analysis, these authors assumed only 2 internal Na^+ ions (for a given line width, τ_I is proportional to N_I), and the intrinsic line width was crudely estimated (*13*). At their frequency of 132 MHz, our MRD analysis indicates that loop and stem ions make comparable contributions to the line width (Figure 3). The single-pulse line width should also include a contribution from chemical shift modulation.

The only prior information about internal ion exchange kinetics in Q3 comes from a ^{1}H NMR study, showing that coexisting Na^+ and K^+ forms are in fast exchange on the ^{1}H chemical shift time scale (*29*). This observation implies that $\tau_{I,loop}$ and $\tau_{I,stem}$ are $\ll$ 10 ms at 25 °C, which is consistent with our results (Table 1).

Ion Selectivity. It has long been known that K^+ has a higher affinity than Na^+ for the internal sites in quadruplexes (*1*). This preference does not result from stronger quadruplex−K^+ interactions, but from the smaller free energy cost of dehydrating the larger K^+ ion (*29, 51*). While it is clear that the K^+ preference pertains to all internal sites in Q3 and Q4 (*10, 29*), quantitative results seem to be available only for Q3. Analysis of the variation of quadruplex ^{1}H chemical shifts as a function of K^+ concentration in the presence of Na^+ thus yielded an equilibrium constant of 3.7−4.6 for exchange of one Na^+ by one K^+ (*29*). This result is in excellent agreement with our exchange constants of 4 for both stem and loop sites (Table 1). For Q4, we find higher selectivity for the stem sites than for the loop sites, but the product $K_{stem}\,K_{loop}$ is the same as for Q3.

The residence times of NH_4^+ and Tl^+ ions at the stem sites is much longer than for Na^+: 250 ms at 10 °C for NH_4^+ at the central site in Q4 (*20*) and 80−155 ms at 25 °C for Tl^+ ions in Q4 (*8*). Moreover, in a mixed NH_4^+/Na^+ form of Q4, the movement of NH_4^+ from the central to the outer stem site was found to be accelerated by a factor 7.5 as compared to the pure NH_4^+ form (*22*). On the basis of these results and model calculations (*52*), it is reasonable to expect that K^+ has substantially longer residence times than Na^+ in the internal sites and that Na^+ exchange (at least from the stem sites) is retarded in mixed Na^+/K^+ forms. The neglect of this complication in our analysis may have affected the parameter values to some extent. However, K^+ ions in the stem sites should not have a large effect on the direct exchange Na^+ ions from the loop sites. Because the ^{23}Na MRD profile is strongly dominated by loop ions in the samples containing KCl (Figure 3), K^+ perturbations of the Na^+ properties should not have a large effect on our analysis.

Hydration Layer Dynamics. It is instructive to compare the present results on the hydration dynamics of the Q3 and Q4 quadruplexes with corresponding results for *B*-DNA oligonucleotides (*32*). In particular, we shall compare the bimolecular DNA dodecamers Q4 and [d(GCGCAATTGCGC)]$_2$ (abbreviated A_2T_2), the latter of which has been studied extensively by ^{2}H and ^{17}O MRD (*16, 17*). In contrast to Q4, A_2T_2 does not give rise to a measurable dispersion at 27 °C (*16*). When scaled to the Q4 concentration (1 mM) and corrected for differences in water isotope composition, the ^{2}H and ^{17}O data for A_2T_2 fall slightly below the dashed α line for Q4 (Figure 2). At 4 °C, a weak dispersion can be discerned for A_2T_2, but the dispersion amplitude is less than 20% of that for Q4 at 27 °C (Figure 2). For A_2T_2, eq 1 thus reduces to $R_1(\omega_0) - R^0 = \alpha$ at 27 °C. With $N_H = 424$, obtained from the solvent-accessible area of A_2T_2, and averaging the ^{2}H and ^{17}O data (which do not differ significantly), we obtain $\xi_H = 3.7 \pm 0.2$ for A_2T_2 at 27 °C. The dynamic perturbation of water dynamics in the hydration layer is therefore ~25% larger for Q4, with $\nu_H = 4.7 \pm 0.6$ (Table 1). This difference may be attributed to the higher charge density of the more compact, nearly spherical Q4 (with 16% smaller solvent-accessible area than A_2T_2). In particular, there may be a substantial contribution from water molecules bridging the closely spaced phosphodiester backbones of the antiparallel strands lining the narrow groove in Q4 (*18, 23*). We note also that the DPFs for Q3 and Q4, $\nu_H = 4.0 \pm 0.5$ and 4.7 ± 0.6, respectively, are in the same range as for the hydration layers of proteins (*43*).

Hydration of Loop Ions. The relaxation dispersion seen for Q4 (and Q3), but not for A_2T_2 (Figure 2), provides conclusive evidence for long-lived hydration water molecules in the quadruplexes. As noted above, there must be at least 2 such water molecules, and they must have residence times in the range 3 ns $\ll \tau_I \ll$ 10 μs at 27 °C. Numerous MRD (*32, 43, 53*) and molecular dynamics simulation (*54, 55*) studies of proteins and nucleic acids have shown that such long-lived water molecules are invariably located in internal cavities or in deep pockets or crevices. In the Q4 quadruplex, such secluded hydration sites exist only in the narrow groove and next to the loop Na^+ ions. The minor groove of the A_2T_2 duplex contains a well-ordered hydration motif known as the spine (*34*), but MRD studies show that even the five most ordered water molecules of the spine, H-bonded to T.O2 and A.N3 atoms at the floor of the deep and narrow groove (*34*), have residence times of only 0.2 ns at 27 °C (*16*). Therefore, even these highly ordered water molecules are not sufficiently long-lived to produce a relaxation dispersion at 27 °C (Figure 2). In contrast to the well-defined spine of hydration in A_2T_2, the hydration motif in the narrow groove of Q4 shows

considerable variation among different quadruplex molecules in the same asymmetric unit and between different crystal forms (*18*). This observation indicates (*18*) that the groove waters in Q4 are more mobile than those in A_2T_2. The relaxation dispersion observed for Q4 (Figure 2) therefore cannot be attributed to groove hydration.

The only plausible location for the long-lived water molecules in the Q4 quadruplex is in direct contact with the loop ions. Crystallographic data on water locations in Q4 are available for one Na^+ quadruplex (PDB entry 1JB7) and for 13 K^+ quadruplexes (PDB entries 1JPQ, 1JRN, 2GWQ and 2GWE). All of the K^+ quadruplexes contain five internal ions: three between the G-quartets and two in the T_4 loops (*18*). The relatively high solvent accessibility of the loop K^+ ions probably accounts for the variability in water coordination of these ions: 54% of the 26 Q4 loop K^+ ions in the PDB archive coordinate two water molecules, 35% coordinate a single water molecule, and 11% have no water ligand. The K^+-O_W distances are in the range 2.6−3.2 Å, comparable to the preferred distance of 2.8 Å in aqueous solution (*56*). In the only crystal structure of the Na^+ form of Q4, both loop ions coordinate a single water molecule at distances of 2.4 and 2.9 Å (*23*). (Crystal interactions break the intrinsic 2-fold symmetry of the Q4 quadruplex.) These Na^+ ions are significantly more buried by the DNA structure than are the corresponding K^+ ions. As a result, the coordinating water molecule is more confined, and there is no space available for a second water ligand. The water ligands of the two loop Na^+ ions are within H-bonding distance of several oxygen atoms, including T6.O2, T7.O2, and an external water molecule. Water molecules in the primary hydration shell of Na^+ ions in aqueous solution exchange on a picosecond time scale (*56*), but, for the water ligands of loop Na^+ ions in Q4, the confined geometry precludes a concerted exchange mechanism where a new water molecule enters as the original one leaves. Rather, the water molecule must exit completely from the deep and narrow passage that connects the Na^+ ion to external solvent before a new water molecule can enter. The energy barrier for water exchange therefore becomes large, leading to a long water residence time.

In aqueous solution, the presence of Na^+ ions in the loops of Q4 is indicated by direct observation of slow-exchange peaks in the ^{23}Na NMR spectrum (*10*). Both the ^{23}Na and ^2H MRD data presented here support this assignment. With $N_I = 2$, the value of $N_I S_I^2$ deduced from the fit to the Q4 data in Figure 2 yields $S_I = 0.88 \pm 0.06$ for the order parameter of this symmetry-related pair of water molecules. This large order parameter is consistent with the additional H-bond interactions of the water ligands (see above), which presumably prevent these water molecules from flipping about their C_2 axes on the time scale (3.5 ns) of quadruplex tumbling. Such fast water flips would have reduced the ^2H dispersion amplitude by a factor 2.7 compared to the ^{17}O amplitude (*39*), but these amplitudes were found to be closely similar.

For Q3, no crystal structure is available. On the basis of the analogy with Q4, it has been argued that Q3 also contains Na^+ ions in the loops (*10*), and our ^{23}Na MRD data support this hypothesis. On the basis of the NMR solution structure of the Na^+ form of Q3 (*25*), it has been proposed (*10*) that the coordination of the loop ions involves, in addition to the four G.O6 atoms of the adjacent G-quartet, two thymine oxygens (T4.O2 and T6.O2) and no water molecule, rather than one thymine oxygen and one water oxygen as in Q4. However, inspection of the NMR structure (1FQP) with Na^+ ions added in the loop sites shows that there is also room for a water molecule in the Na^+ coordination sphere. Like the water ligands of the loop Na^+ ions in Q4 (crystal structure 1JB7), the putative water ligands in Q3 are geometrically confined, but the H-bond partners are different in Q3 (T7.O2 and possibly T4.N3). For the same reason as for Q4, the grooves of Q3 are not likely to contain long-lived water (*28*). We therefore attribute the ^2H dispersion for Q3 (Figure 2) to water ligands of the loop ions, just as for Q4. With $N_I = 2$, the value of $N_I S_I^2$ deduced from the fit to the Q3 data in Figure 2 yields $S_I = 0.93 \pm 0.05$ for the root-mean-square order parameter of these two nonsymmetry-related water molecules.

CONCLUSIONS

We have presented here the first MRD study of quadruplex DNA, using $^2H/^{17}O$ spin relaxation to probe water dynamics and ^{23}Na relaxation to probe the internal Na^+ ions in two diagonal-looped foldback quadruplexes in aqueous solution at 27 °C. The principal conclusions of this study are as follows.

(1) Water ^2H and ^{17}O dispersions are observed for both Q3 and Q4, implying at least two water molecules with residence times in the range 3 ns $\ll \tau_I \ll$ 10 μs. The only plausible location for these water molecules is as ligands to Na^+ ions in the loop sites, as seen in the crystal structure of Q4 (*23*). The water MRD data thus indicate that both Q3 and Q4 contain loop ions with one water ligand. The high orientational order parameter of these water ligands, $S_I \approx 0.9$, is consistent with their involvement in multiple H-bonds (*23*).

(2) Water rotation in the hydration layer on the quadruplex surface is slowed down by a factor 4.0 ± 0.5 for Q3 and 4.7 ± 0.6 for Q4. This dynamic perturbation factor is similar to that of small proteins (4.2 ± 0.4) but larger than that of a *B*-DNA duplex with an ordered spine of hydration in the minor groove (3.7 ± 0.2). Water molecules bridging phosphate groups across the narrow groove of the quadruplexes may make a disproportionate contribution to the global dynamic perturbation factor, but all external water molecules exhibit subnanosecond dynamics.

(3) The extended shape of the ^{23}Na dispersions observed for both quadruplexes indicates two classes of long-lived Na^+ ions. One of these classes must be in the slow-exchange regime, with residence times of ~1 ms so that the effective correlation time becomes much shorter than the 3−4 ns tumbling time of the quadruplex. The other class is in the fast-to-intermediate exchange regime, with residence times <100 μs.

(4) The slowly exchanging ion class is assigned to sites between each pair of G-quartets in the quadruplex stem. With three such sites in Q4, the QCC derived from the MRD data agrees quantitatively with that determined by solid-state ^{23}Na NMR (*24*). The MRD data thus support the view (*10*) that Q4 contains five internal Na^+ ions in roughly the same locations as the K^+ ions seen in crystal structures of Q4 (*18*). For Q3, we find a larger QCC, indicating a less symmetric

coordination, as would be the case if the Na^+ ions prefer locations closer to one of the adjacent G-quartets. For both Q3 and Q4, the Na^+ ions in the stem sites have residence times in the range 0.6−1.0 ms.

(5) The more rapidly exchanging ion class is assigned to the loop sites, the existence of which is also indicated by the ^2H MRD data. This finding supports the proposal, based on ^{23}Na NMR spectroscopy and structural data, that all diagonal foldback quadruplexes bind Na^+ ions in the loops (*10*). The residence times of these ions are not accurately determined by the MRD data but appear to be in the range 10−60 μs at 27 °C and in the presence of 220 mM Na^+. The smaller QCCs deduced for the loop ions can be explained by averaging over multiple coordination geometries, perhaps involving both six and seven ligands, which are accessed on time scales shorter than a few ns.

(6) For both quadruplexes, K^+ ions bind to stem and loop sites with higher affinity than Na^+ ions, as expected from the higher melting temperature of the K^+ form (*36, 38*). The product of the equilibrium exchange constants is ∼16 for both quadruplexes. For Q3, the individual exchange constants are ∼4, in agreement with results derived from ^1H chemical shift titrations (*29*).

ACKNOWLEDGMENT

We thank Vladimir Denisov and Hans Lilja for assistance with NMR spectrometers and Stuart Allison for advice on electrolyte friction.

REFERENCES

1. Williamson, J. R. (1994) G-quartet structures in telomeric DNA. *Annu. Rev. Biophys. Biomol. Struct. 23*, 703–730.
2. Neidle, S., and Balasubramanian, S., Eds. (2006) *Quadruplex Nucleic Acids*, The Royal Society of Chemistry, Cambridge, U.K.
3. Maizels, N. (2006) Dynamic roles for G4 DNA in the biology of eukaryotic cells. *Nat. Struct. Mol. Biol. 13*, 1055–1059.
4. Davis, J. T. (2004) G-quartets 40 years later: From 5′-GMP to molecular biology and supramolecular chemistry. *Angew. Chem., Int. Ed. 43*, 668–698.
5. Hardin, C. C., Perry, A. G., and White, K. (2001) Thermodynamic and kinetic characterization of the dissociation and assembly of quadruplex nucleic acids. *Biopolymers 56*, 147–194.
6. Hud, N. V., Ed. (2008) *Nucleic Acid - Metal Ion Interactions*, The Royal Society of Chemistry, Cambridge, U.K.
7. Hud, N. V., Schultze, P., and Feigon, J. (1998) Ammonium ion as an NMR probe for monovalent cation coordination sites of DNA quadruplexes. *J. Am. Chem. Soc. 120*, 6403–6404.
8. Gill, M. L., Strobel, S. A., and Loria, J. P. (2005) ^{205}Tl NMR methods for the characterization of monovalent cation binding to nucleic acids. *J. Am. Chem. Soc. 127*, 16723–16732.
9. Wong, A., Ida, R., and Wu, G. (2005) Direct NMR detection of the "invisible" alkali metal cations tightly bound to G-quadruplex structures. *Biochem. Biophys. Res. Commun. 337*, 363–366.
10. Ida, R., and Wu, G. (2008) Direct NMR detection of alkali metal ions bound to G-quadruplex DNA. *J. Am. Chem. Soc. 130*, 3590–3602.
11. Borzo, M., Detellier, C., Laszlo, P., and Paris, A. (1980) ^1H, ^{23}Na, and ^{31}P NMR studies of the self-assembly of the 5′-guanosine monophosphate dianion in neutral aqueous solution in the presence of sodium cations. *J. Am. Chem. Soc. 102*, 1124–1134.
12. Xu, Q., Deng, H., and Braunlin, W. H. (1993) Selective localization and rotational immobilization of univalent cations on quadruplex DNA. *Biochemistry 32*, 13130–13137.
13. Deng, H., and Braunlin, W. H. (1996) Kinetics of sodium ion binding to DNA quadruplexes. *J. Mol. Biol. 255*, 476–483.
14. Denisov, V. P., and Halle, B. (2000) Sequence-specific binding of counterions to *B*-DNA. *Proc. Natl. Acad. Sci. U.S.A. 97*, 629–633.
15. Cesare Marincola, F., Denisov, V. P., and Halle, B. (2004) Competitive Na^+ and Rb^+ binding in the minor groove of DNA. *J. Am. Chem. Soc. 126*, 6739–6750.
16. Denisov, V. P., Carlström, G., Venu, K., and Halle, B. (1997) Kinetics of DNA hydration. *J. Mol. Biol. 268*, 118–136.
17. Jóhannesson, H., and Halle, B. (1998) Minor groove hydration of DNA in solution: Dependence on base composition and sequence. *J. Am. Chem. Soc. 120*, 6859–6870.
18. Haider, S., Parkinson, G. N., and Neidle, S. (2002) Crystal structure of the potassium form of an *Oxytricha nova* G-quadruplex. *J. Mol. Biol. 320*, 189–200.
19. Gill, M. L., Strobel, S. A., and Loria, J. P. (2006) Crystallization and characterization of the thallium form of the *Oxytricha nova* G-quadruplex. *Nucleic Acids Res. 34*, 4506–4514.
20. Hud, N. V., Schultze, P., Sklenár, V., and Feigon, J. (1999) Binding sites and dynamics of ammonium ions in a telomere repeat DNA quadruplex. *J. Mol. Biol. 285*, 233–243.
21. Schultze, P., Hud, N. V., Smith, F. W., and Feigon, J. (1999) The effect of sodium, potassium and ammonium ions on the conformation of the dimeric quadruplex formed by the *Oxytricha nova* telomere repeat oligonucleotide $d(G_4T_4G_4)$. *Nucleic Acids Res. 27*, 3018–3028.
22. Sket, P., Crnugelj, M., Kozminski, W., and Plavec, J. (1970) (2004) $^{15}NH_4^+$ ion movement inside $d(G_4T_4G_4)_2$ G-quadruplex is accelerated in the presence of smaller Na^+ ions. *Org. Biomol. Chem. 2* 1973.
23. Horvath, M. P., and Schultz, S. C. (2001) DNA G-quartets in a 1.86 Å resolution structure of an *Oxytricha nova* telomeric protein-DNA complex. *J. Mol. Biol. 310*, 367–377.
24. Wu, G., and Wong, A. (2004) Solid-state ^{23}Na NMR determination of the number and coordination of sodium cations bound to *Oxytricha nova* telomere repeat $d(G_4T_4G_4)$. *Biochem. Biophys. Res. Commun. 323*, 1139–1144.
25. Keniry, M. A., Strahan, G. D., Owen, E. A., and Shafer, R. H. (1995) Solution structure of the Na^+ form of the dimeric guanine quadruplex $[d(G_3T_4G_3)]_2$. *Eur. J. Biochem. 233*, 631–643.
26. Scaria, P. V., Shire, S. J., and Shafer, R. H. (1992) Quadruplex structure of $d(G_3T_4G_3)$ stabilized by K^+ or Na^+ is an asymmetric hairpin dimer. *Proc. Natl. Acad. Sci. U.S.A. 89*, 10336–10340.
27. Smith, F. W., Lau, F. W., and Feigon, J. (1994) $d(G_3T_4G_3)$ forms an asymmetric diagonally looped dimeric quadruplex with guanosine 5′-*syn*-*syn*-*anti* and 5′-*syn*-*anti*-*anti* N-glycosidic conformations. *Proc. Natl. Acad. Sci. U.S.A. 91*, 10546–10550.
28. Strahan, G. D., Keniry, M. A., and Shafer, R. H. (1998) NMR structure refinement and dynamics of the K^+-$[d(G_3T_4G_3)]_2$ quadruplex via particle mesh Ewald molecular dynamics simulations. *Biophys. J. 75*, 968–981.
29. Hud, N. V., Smith, F. W., Anet, F. A. L., and Feigon, J. (1996) The selectivity for K^+ versus Na^+ in DNA quadruplexes is dominated by relative free energies of hydration: A thermodynamic analysis by ^1H NMR. *Biochemistry 35*, 15383–15390.
30. Smith, F. W., and Feigon, J. (1993) Strand orientation in the DNA quadruplex formed from the *Oxytricha* telomere repeat oligonucleotide $d(G_4T_4G_4)$ in solution. *Biochemistry 32*, 8682–8692.
31. Berman, H. M., and Schneider, B. (1998) Nucleic acid hydration, in *Handbook of Nucleic Acid Structure* (Neidle, S., Ed.) pp 295−312, Oxford University Press, Oxford, U.K.
32. Halle, B., and Denisov, V. P. (1998) Water and monovalent ions in the minor groove of B-DNA oligonucleotides as seen by NMR. *Biopolymers 48*, 210–233.
33. Jayaram, B., and Jain, T. (2004) The role of water in protein-DNA recognition. *Annu. Rev. Biophys. Biomol. Struct. 33*, 343–361.
34. Tereshko, V., Minasov, G., and Egli, M. (1999) The Dickerson-Drew B-DNA dodecamer revisited at atomic resolution. *J. Am. Chem. Soc. 121*, 470–471.
35. Cantor, C. R., Warshaw, M. M., and Shapiro, H. (1970) Oligonucleotide interactions. III. Circular dichroism studies of the conformation of deoxyoligonucleotides. *Biopolymers 9*, 1059–1077.
36. Lu, M., Guo, Q., and Kallenbach, N. R. (1993) Thermodynamics of G-tetraplex formation by telomeric DNAs. *Biochemistry 32*, 598–601.
37. Petraccone, L., Erra, E., Esposito, V., Randazzo, A., Mayol, L., Nasti, L., Barone, G., and Giancola, C. (2004) Stability and structure of telomeric DNA sequences forming quadruplexes containing four G-tetrads with different topological arrangements. *Biochemistry 43*, 4877–4884.
38. Dapic, V., Abdomerovic, V., Marrington, R., Peberdy, J., Rodger, A., Trent, J. O., and Bates, P. J. (2097) (2003) Biophysical and biological properties of quadruplex oligodeoxyribonucleotides. *Nucleic Acids Res. 31*, 2107.

39. Halle, B., Denisov, V. P., and Venu, K. (1999) Multinuclear Relaxation Dispersion Studies of Protein Hydration, in *Biological Magnetic Resonance* (Krishna, N. R., and Berliner, L. J., Eds.) pp 419−484, Kluwer Academic Plenum, New York.
40. Fernandes, M. X., Ortega, A., LópezMartínez, M. C., and Garciade la Torre, J. (2002) Calculation of the hydrodynamic properties of small nucleic acids from their atomic structure. *Nucleic Acids Res. 30*, 1782–1788.
41. Halle, B., and Davidovic, M. (2003) Biomolecular hydration: From water dynamics to hydrodynamics. *Proc. Natl. Acad. Sci. U.S.A. 100*, 12135–12140.
42. Schultze, P., Smith, F. W., and Feigon, J. (1994) Refined solution structure of the dimeric quadruplex formed from the *Oxytricha* telomeric oligonucleotide d(GGGGTTTTGGGG). *Structure 2*, 221–233.
43. Mattea, C., Qvist, J., and Halle, B. (2008) Dynamics at the protein-water interface from ^{17}O spin relaxation in deeply supercooled solutions. *Biophys. J. 95*, 2951–2963.
44. Korolev, N., Lyubartsev, A. P., Laaksonen, A., and Nordenskiöld, L. (2002) On the competition between water, sodium ions, and spermine in binding to DNA: A molecular dynamics computer simulation study. *Biophys. J. 82*, 2860–2875.
45. Wong, A., and Wu, G. (2000) Solid-state ^{23}Na nuclear magnetic resonance of sodium complexes with crown ethers, cryptands, and naturally occurring antibiotic ionophores: A direct probe to the sodium-binding sites. *J. Phys. Chem. A 104*, 11844–11852.
46. Wong, A., and Wu, G. (2003) Characterization of the pentacoordinate sodium cations in the hydrated nucleoside 5′-phosphates by solid-state ^{23}Na NMR and quantum mechanical calculations. *J. Phys. Chem. A 107*, 579–586.
47. Halle, B. (2004) Biomolecular cryocrystallography: Structural changes during flash-cooling. *Proc. Natl. Acad. Sci. U.S.A. 101*, 4793–4798.
48. Cevec, M., and Plavec, J. (2005) Role of loop residues and cations on the formation and stability of dimeric DNA G-quadruplexes. *Biochemistry 44*, 15238–15246.
49. Dingley, A. J., Peterson, R. D., Grzesiek, S., and Feigon, J. (2005) Characterization of the cation and temperature dependence of DNA quadruplex hydrogen bond properties using high-resolution NMR. *J. Am. Chem. Soc. 127*, 14466–14472.
50. Goel, N. S., and Richter-Dyn, N. (1974) *Stochastic Models in Biology*, Academic Press, New York.
51. Gu, J., and Leszczynski, J. (2002) Origin of Na^+/K^+ selectivity of the guanine tetraplexes in water: The theoretical rationale. *J. Phys. Chem. A 106*, 529–532.
52. van Mourik, T., and Dingley, A. J. (2005) Characterization of the monovalent ion position and hydrogen-bond network in guanine quartets by DFT calculations and NMR parameters. *Chem.—Eur. J. 11*, 6064–6079.
53. Denisov, V. P., and Halle, B. (1996) Protein hydration dynamics in aqueous solution. *Faraday Discuss. 103*, 227–244.
54. Makarov, V. A., rews, B. K., Smith, P. E., and Pettitt, B. M. (2000) Residence times of water molecules in the hydration sites of myoglobin. *Biophys. J. 79*, 2966–2974.
55. Henchman, R. H., and McCammon, J. A. (2002) Structural and dynamic properties of water around acetylcholinesterase. *Protein Sci. 11*, 2090.
56. Ohtaki, H., and Radnai, T. (1993) Structure and dynamics of hydrated ions. *Chem. Rev. 93*, 1157–1204.

BI801657S